*Molecular Physics*, Vol. 104, Nos. 16–17, 20 August–10 September 2006, 2801–2814

Taylor & Francis
Taylor & Francis Group

# *Ab initio* spectroscopy of $D_2H^+$ near dissociation

PAOLO BARLETTA, BRUNO C. SILVA,
JAMES J. MUNRO and JONATHAN TENNYSON*

Department of Physics and Astronomy, University College London,
Gower St., London WC1E 6BT, UK

(*Received 25 January 2006; in final form 14 June 2006*)

Extensive calculations for the vibrational band origins of $D_2H^+$ up to dissociation are presented. Due to the high density of vibrational states near dissociation, huge basis sets needed to be used as well as massively parallel computers. We have found 1209 $A_1$ and 1078 $B_1$ bound states, some of which display long-range features, which are analysed in detail. The calculations were performed within the Born–Oppenheimer approximation and non-adiabatic corrections to it are evaluated. However, the main source of error for the states near dissociation arises from the Potential Energy Surface at high energies.

*Keywords*: *Ab initio* spectroscopy; $D_2H^+$; Vibrational states

## 1. Introduction

The study of chemically bound polyatomic molecular systems close to their dissociation limit presents considerable computational challenges. This is due to the number of bound states which are supported by normal molecular interaction and the fact that the characteristics of highly excited states must be very different from those of the lower states. In fact, one might expect states which approach dissociation to exhibit features suggestive of dissociation, such as very long-range extension. For example, in the region of the potential which lies in the energy range between the classical and the quantum dissociation limit there is no constraint on the extent of the molecule other than that due to zero point effects in the dissociation products. The inherent computational difficulties associated with theoretical studies on such states means that there are relatively few studies which investigate vibrational–rotational levels near dissociation for chemically bound species.

The $H_3^+$ molecule (and its isotopologues) represent a benchmark system for chemical physics [1]. It is the (electronically) simplest bound polyatomic molecule, having only two electrons and three nuclei, and it is possible to compute its ground electronic surface very accurately up to dissociation [2]. Furthermore, $H_3^+$ has an important role in astronomy, as it has been discovered to be an active component of both the diffuse and dense interstellar medium, and the ionospheres of giant planets such as Jupiter [3]. Finally, an important series of experiments by Carrington and co-workers [4–6] characterized the infra-red near-dissociation spectrum of $H_3^+$ and its isotopologues. These observations remain largely unexplained by theory but have fueled a considerable number of publications on the subject [7–10]. Although the main focus of their experiments was on $H_3^+$, Carrington and co-workers also studied the deuterated isotopologues $D_3^+$, $H_2D^+$ and $D_2H^+$. They found that the $D_3^+$ spectrum was essentially similar to the $H_3^+$ spectrum, whereas the mixed-isotope species displayed additional features. Of the two mixed isotopologues, the spectrum of $D_2H^+$ was studied in greater detail as its fragments were easier to detect.

Munro *et al*. [9, 11] performed calculations on the near dissociation vibrational states of $H_3^+$; they highlighted the characteristics of a particular set of states lying close to the dissociation limit, whose wavefunctions had a significant amplitude for large values of the dissociating coordinate. Those states were called asymptotic vibrational states (AVS). In the present work, we study the near dissociation vibrational spectrum of $D_2H^+$ and compare the spectra of the two isotopologues by computing also the expectation values for a number of observables, including the rotational constants, in order to obtain a deeper understanding of the properties of those states.

*Corresponding author. Email: j.tennyson@ucl.ac.uk

*Molecular Physics*
ISSN 0026–8976 print/ISSN 1362–3028 online 
http://www.tandf.co.uk/journals
DOI: 10.1080/00268970600868641

This paper is organized as follows. In section 2, we present and discuss details of our calculations for the bound states of $D_2H^+$. In section 3, we present the results, including an extensive listing of the vibrational states close to the dissociation limit. In section 4, corrections to the non-relativistic Born–Oppenheimer (BO) Hamiltonian are discussed and evaluated qualitatively. The final section is devoted to the conclusions.

## 2. Calculations

The Potential Energy Surface (PES) used in the present calculation is the PPKT2 potential [9]. This is the fully *ab initio* PES of Polyansky *et al*. [2] adjusted to remove a non-physical hump at large values of the dissociating coordinate [12]. In the present calculations we neglect corrections to the non-relativistic BO framework, as those corrections are likely to be much smaller than the residual error in the potential in the near-dissociation region, although it should be noted that the Born–Oppenheimer corrections for $D_2H^+$ have a lower symmetry than the potential [13]. The effects of these have been evaluated perturbatively and are discussed in section 4.

The minimum of the PPKT2 PES is given by an equilateral triangle of sides $1.65a_0$. The classical dissociation channel is open at an energy of $37\,169.4\,\mathrm{cm}^{-1}$ above the minimum of the potential, and corresponds to a process of the kind $X_3^+ \rightarrow X_2 + X^+$. We shall refer to this value as $D_e$. The asymptotic interaction between the diatom and the ion fragment is given, to first order [14], by the charge-induced dipole and charge-quadrupole, whose leading term is of the order $\approx 1/R^3$, where $R$ is the dissociation coordinate. For $D_2H^+$, due to the presence of two isotopic species, two different break-up processes can occur. Figure 1 shows different cuts through the PES, and illustrates the break-up reactions possible. Those reactions have different dissociation energies ($D_0$) as a result of the different zero-point energies of the diatomic fragments. The energy region between the opening of the dissociation channel and the zero-point energy of the diatomic fragment is very interesting. Classical states in this energy range can dissociate but quantum mechanical states are bound by the zero-point energy of their constituents [15]. In this region, the system does not have enough energy to dissociate, but its size could be very large as there is no potential barrier in the $R$ coordinate. In fact, one might expect the bound three-body states lying in this energy range to display strong features suggestive of dissociation, such as very extended wave functions.

For the $D_2H^+$ $J=0$ bound states calculation we follow the work of Munro *et al*. [9]. We will report below only the main details of the procedure. Two-body nuclear motion calculations were performed using the LEVEL code [16] to characterize the zero-point energies of the various dissociation products. The values of 1.0075372 u and 2.013814 u were used for the H and D nuclei masses, as recommended in [17]. The best values for these masses is discussed in section 4. Three-body calculations were performed using an adapted version of the PDVR3D [18] program. This program employs a three-dimensional DVR scheme to solve the nuclear motion problem within the Born–Oppenheimer approximation for the ground electronic potential energy surface. We have used Radau coordinates [19] to parametrize the three internal degrees of freedom of the molecule, and the associated DVR was based on spherical oscillators for the two radial coordinates $(r_1, r_2)$ and Legendre polynomials for the angular coordinate $\alpha$. However, for sake of clarity, in all the figures we have used Jacobi coordinates $(r, R, \theta)$ to represent the wavefunctions, as their physical interpretation is much more immediate than for the Radau coordinates. In Jacobi coordinates, $r$ is the diatom internuclear distance, $R$ is the distance between the centre of mass of the diatom and the third particle, and $\theta$ represents the angle between $r$ and $R$.

To converge an extended number of levels for $D_2H^+$ (up to the lowest dissociation channel) a vast basis set is required. The PDVR3D code can exploit the $C_{2v}$ symmetry of the problem. Therefore, a complete calculation is done by indicating explicitly the symmetry of the diatom pair, which can be $A_1$ or $B_1$, and then repeating the calculation for each symmetry. The final basis set included 120 points for each radial coordinate, and 96 points of the angular coordinate. The radial basis set was constructed from spherical oscillators [20] with $w_e = 0.004$ Hartree, and $\alpha = 0$, and covers the range from 0.09 to $12.80a_0$. The convergence of our results was checked against variation of all the basis set parameters mentioned above, also following the experience gained in [9]. Whereas for the angular grid the range is fixed, for the radial grid we have varied both the number of points and the grid extension, as shown in the footnote of table 1. The radial grid range is in Radau coordinates, and corresponds to a range of about $0–20a_0$ in the dissociating coordinate $R$.

Table 1 shows the convergence for the highest five $A_1$ bound states as a function of the number of radial points $N_r$, angular points $N_\alpha$ and the 2D cutoff $E_{2D}$. The convergence is shown for the energy $E$, the rotational constant $C$, and the mean value of the dissociating coordinate $\langle R \rangle$. As expected for a (pseudo-)variational method, the convergence is much better for the energy than for the other observables. It is not simple to quantify the absolute precision of our calculation as it

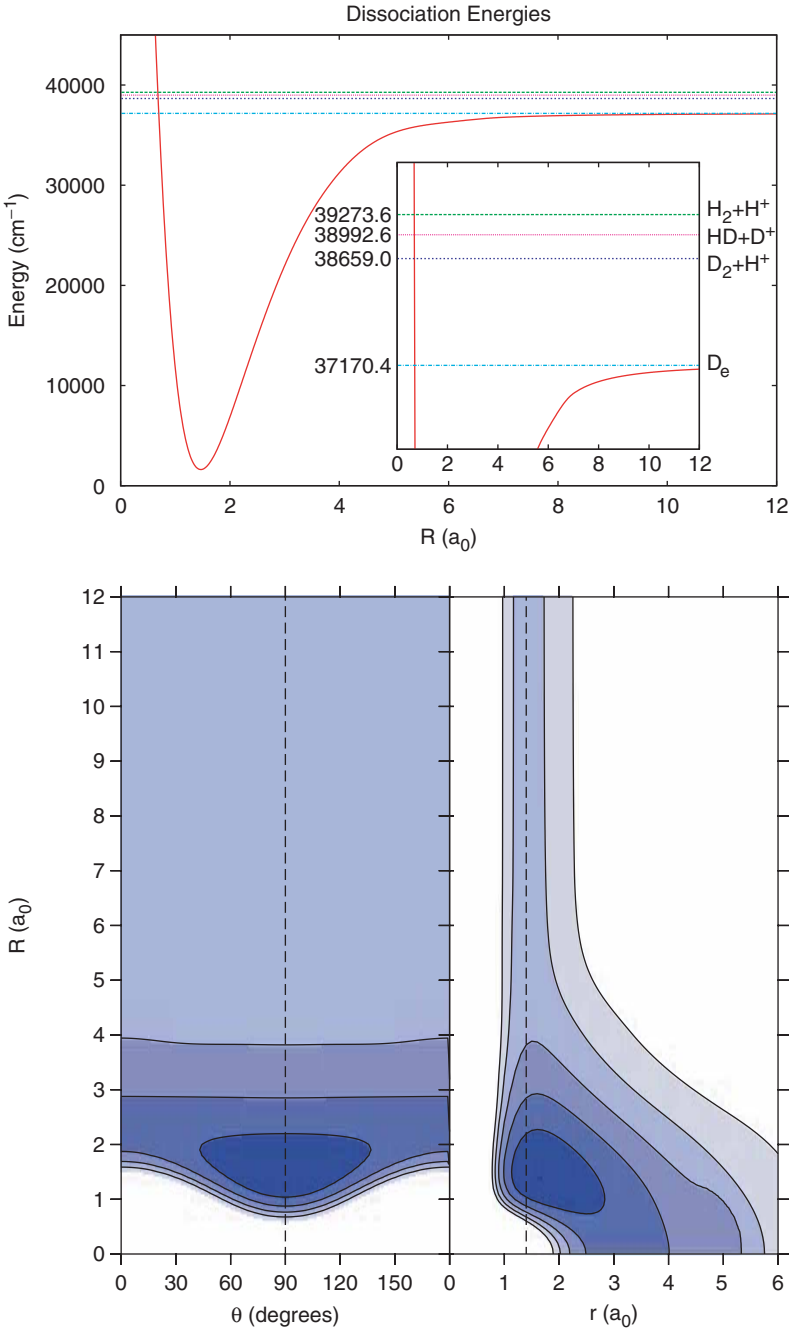


Figure 1. Cuts through the potential energy surface. The potential surface is represented for sake of clarity in Jacobi coordinates $\{r, R, \theta\}$, where $r$ is the diatom distance, $R$ is the distance between the third particle and the diatom centre of mass, and $\theta$ is the relative angle. In the bottom plot, two three-dimensional cuts $V(1.411, R, \theta)$ and $V(r, R, 90)$ are presented. The depth of the potential is represented using contour lines of interval $10^4\,\mathrm{cm}^{-1}$. The dashed line represents the collocation of the two-dimensional cut of the right-hand picture. The upper plot shows the dissociation channel $V(1.411, R, 90)$ of the PES along with the lowest dissociative reactions for both $H_3^+$ and $D_2H^+$.

depends on the many factors mentioned above. It can be noted from table 1 that the various errors tend to cancel each other. However, we can say that the overall convergence of the energy averaged for all calculated levels is within $0.1\,\mathrm{cm}^{-1}$, except for the last state (number 1209), for which the convergence is of the order $1\,\mathrm{cm}^{-1}$. Due to the computational cost of each job we have not repeated a similar convergence study for the $B_1$ bound states, and we assumed that the basis set found to be the best for the $A_1$ states would provide a

Table 1. Convergence of the energy $E$, the rotational constant $C$ and the mean value of the dissociative coordinate $\langle R \rangle$ for the highest five even parity band origins (states 1205–1209) for $D_2H^+$ with respect to changes in the basis set size and the cut-off parameter. The values in columns $E$, $C$ and $R$ refer to the basis sets described in the text, whereas the differences are the converged values minus the values with the indicated basis set. Units are $cm^{-1}$ for $E$ and $C$, $a_0$ for $R$.

| $N_e$ | $E$ | $\Delta E^a$ | $\Delta E^b$ | $\Delta E^c$ | $C$ | $\Delta C^a$ | $\Delta C^b$ | $\Delta C^c$ | $R$ | $\Delta R^a$ | $\Delta R^b$ | $\Delta R^c$ |
|---|---|---|---|---|---|---|---|---|---|---|---|---|
| 1205 | 38 632.901 | −0.008 | 0.007 | −0.130 | 7.984 | 0.007 | 0.009 | 0.018 | 4.578 | 0.003 | 0.005 | 0.010 |
| 1206 | 38 633.914 | −0.027 | 0.001 | −0.081 | 9.334 | −0.012 | −0.001 | −0.013 | 5.281 | −0.006 | 0.000 | −0.006 |
| 1207 | 38 640.219 | −0.011 | 0.028 | −0.094 | 7.542 | −0.022 | 0.034 | −0.004 | 4.333 | −0.013 | 0.019 | −0.002 |
| 1208 | 38 649.775 | −0.151 | 0.242 | −0.071 | 6.149 | −0.227 | 0.380 | 0.017 | 3.536 | 0.128 | 0.343 | 0.137 |
| 1209 | 38 655.445 | −0.395 | 0.551 | −0.052 | 6.266 | −0.131 | 0.101 | −0.026 | 3.581 | −0.075 | 0.059 | −0.015 |

[a] $N_r = 110$ (0.09–12.23$a_0$), $N_\alpha = 96$, $E_{2D} = 72\,689.84\,cm^{-1}$.
[b] $N_r = 120$ (0.09–12.80$a_0$), $N_\alpha = 88$, $E_{2D} = 72\,689.84\,cm^{-1}$.
[c] $N_r = 120$ (0.09–12.80$a_0$), $N_\alpha = 96$, $E_{2D} = 70\,577.38\,cm^{-1}$.

similar accuracy for the $B_1$ states, as there is a lower density of states for this symmetry. Convergence for the lower-lying states was found to be very significantly better than for those tabulated, which are the highest considered in our study. This is a general feature of variational methods.

As a result, the final grid contained 696 960 points in the $A_1$ symmetry and 685 440 points in the $B_1$ symmetry. The implementation of the DVR method leads to the diagonalization of a real symmetric matrix which characterizes the eigenvalue problem. In order to obtain eigenvalues and eigenvectors of such a vast matrix we have used a truncation-diagonalization approach [21, 22]. For each angular point the associated 2D sub-matrix was diagonalized, and only those 2D eigenstates with energy less than a chosen cutoff $E_{2D}$ were retained. The value of $E_{2D}$ was then chosen to give a convergence error of less than $0.2\,cm^{-1}$. The dimension of the final 3D matrix was of 121 999 (17.5% of the original basis set), corresponding to $E_{2D} = 72\,689.84\,cm^{-1}$. The calculations were performed on the HPC*x* supercomputer at the Daresbury Laboratory, UK, and required 864 processors for 4 h 13 min. We used as a diagonalizer the routine PDSYEVD from the ScaLAPACK library (http://www.netlib.org/scalapack/).

The $D_2H^+$ problem proved to be numerically more demanding than $H_3^+$; this is due to the higher density of bound states of the former with respect to the latter. As an example, if one considers the energy range between $D_e$ and dissociation, $H_3^+$ has 120 states in an interval of $2100\,cm^{-1}$, whereas $D_2H^+$ shows 181 states in an interval of about $1500\,cm^{-1}$. We obtained a total of 2287 bound states for $D_2H^+$ (1209 $A_1$, 1078 $B_1$), which represents, by the variational principle, a lower limit on the actual number supported by the PPKT2 potential. Equivalent calculations on $H_3^+$ gave 859 states. This number is reduced with respect to $D_2H^+$ not only by mass effects but also by the higher symmetry of the $H_3^+$ isotopologue, as degenerate states are not counted twice.

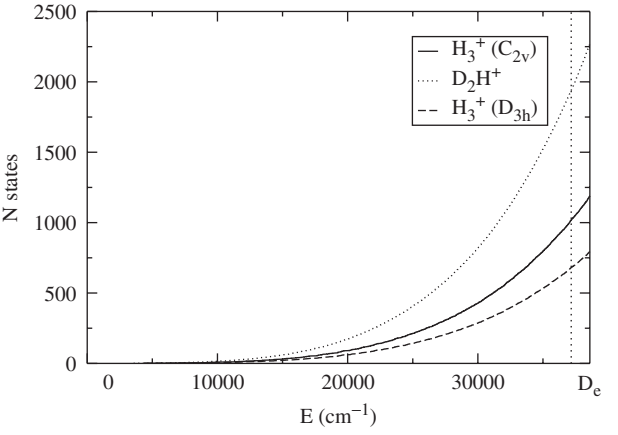


Figure 2. Number of vibrational bound states for $H_3^+$ with standard $D_{3h}$ symmetry and lower ($C_{2v}$) symmetry, and $D_2H^+$, up to dissociation given by $D_0(D_2H^+)$.

Figure 2 shows these effects by comparing the density of $H_3^+$ in the 'proper' $D_{3h}$ symmetry, $H_3^+$ in a $C_{2v}$ symmetry, and $D_2H^+$. Application of the Pauli principle would lead to a further reduction as $H_3^+$ states of $A_1$ symmetry are forbidden.

The DVR approach also gives an approximation for the wavefunction of all bound states as eigenvectors of the Hamiltonian matrix. Using these eigenvectors we have calculated the mean value of a range of observables, including some geometric ones, such as the distance between the various particles, or the included angles, and kinetic ones, like the potential energy. Another observable of interest is the rotational constant $C$ associated with the in-plane motion of the molecule. For our purposes this constant is defined by the mean value of the inverse of the molecules moment of inertia and computed using the method of Ernesti and Hudson [23], which is designed for floppy molecules. Such constants have been found useful for other floppy systems [24]. All the integrals associated with the

calculation of the mean values have been evaluated using the DVR approximation.

## 3. Results

Tables 2 and 3 present the converged values of the energy for those levels above the $D_e$ threshold, for levels of $A_1$ and $B_1$ symmetry, respectively. The mean values of the inter-diatom distance $r$ and the diatom–ion distance $R$, where the diatom is constituted by $D_2$, as well as the D–H–D angle $\gamma$ and the H–D–D angle $\beta$, are also shown to help in characterizing the geometrical features of the states, as well as the rotational constant $C$, and the mean potential energy.

In order to show how the properties of high-lying states differ from those of lower-lying states, the tables also include results for the lowest four states for each symmetry and some of the intermediate states. There are several differences one can immediately recognize between the lower and upper part of the spectrum: the rotational constant for the high-lying states is less than half its value for the ground state. This last character is

Table 2. Energy levels of $A_1$ symmetry for $D_2H^+$. Units are $cm^{-1}$ for $E$, $C$ and $V$, $a_0$ for $r$ and $R$, degrees for $\beta$ and $\gamma$.

| $n$ | $E$ | $\langle R\rangle$ | $\langle r\rangle$ | $\langle\beta\rangle$ | $\langle\gamma\rangle$ | $C$ | $\langle V\rangle$ | $n$ | $E$ | $\langle R\rangle$ | $\langle r\rangle$ | $\langle\beta\rangle$ | $\langle\gamma\rangle$ | $C$ | $\langle V\rangle$ |
|---|---|---|---|---|---|---|---|---|---|---|---|---|---|---|---|
| 1 | 3561.76 | 1.49 | 1.70 | 60.53 | 59.90 | 12.96 | 1824.19 | 2 | 5529.21 | 1.46 | 1.79 | 58.90 | 63.87 | 12.32 | 2872.93 |
| 3 | 6299.46 | 1.55 | 1.72 | 61.22 | 58.81 | 12.58 | 3289.43 | 4 | 7381.59 | 1.44 | 1.87 | 57.53 | 67.41 | 11.75 | 3923.94 |
| 43 | 15 777.81 | 1.58 | 2.04 | 58.55 | 68.50 | 10.06 | 8965.28 | 44 | 15 825.30 | 1.92 | 1.76 | 70.98 | 47.43 | 9.98 | 9809.01 |
| 245 | 25 600.81 | 1.82 | 2.29 | 63.08 | 67.49 | 7.94 | 15 800.07 | 246 | 25 603.88 | 2.03 | 2.11 | 67.44 | 55.90 | 8.51 | 15 559.81 |
| 631 | 32 846.80 | 2.25 | 2.40 | 67.71 | 60.65 | 6.47 | 20 643.77 | 632 | 32 849.30 | 2.22 | 2.44 | 67.92 | 59.64 | 6.51 | 20 194.59 |
| 1029 | 37 181.90 | 2.30 | 2.58 | 64.53 | 66.56 | 6.00 | 23 240.74 | 1030 | 37 191.29 | 2.28 | 2.59 | 66.40 | 62.54 | 6.06 | 23 076.95 |
| 1031 | 37 204.01 | 2.53 | 2.36 | 70.85 | 53.66 | 6.07 | 23 025.64 | 1032 | 37 212.10 | 2.26 | 2.67 | 65.18 | 66.67 | 5.78 | 23 330.68 |
| 1033 | 37 219.34 | 2.50 | 2.46 | 69.29 | 57.72 | 5.90 | 23 390.58 | 1034 | 37 223.92 | 2.21 | 2.71 | 64.18 | 68.32 | 5.87 | 23 305.76 |
| 1035 | 37 241.67 | 2.19 | 2.69 | 63.51 | 69.19 | 5.97 | 23 058.25 | 1036 | 37 242.82 | 2.45 | 2.55 | 68.23 | 59.33 | 5.96 | 23 718.43 |
| 1037 | 37 252.07 | 2.21 | 2.72 | 63.52 | 69.68 | 5.73 | 23 558.93 | 1038 | 37 256.80 | 2.49 | 2.50 | 68.56 | 59.64 | 5.73 | 23 893.66 |
| 1039 | 37 270.29 | 2.25 | 2.68 | 64.69 | 66.36 | 5.95 | 23 559.91 | 1040 | 37 275.97 | 2.41 | 2.50 | 67.87 | 60.52 | 6.00 | 23 394.99 |
| 1041 | 37 281.09 | 2.29 | 2.65 | 65.00 | 66.35 | 5.82 | 23 883.74 | 1042 | 37 306.01 | 2.35 | 2.56 | 66.90 | 61.63 | 6.06 | 23 278.30 |
| 1043 | 37 311.98 | 2.42 | 2.47 | 67.71 | 60.49 | 5.91 | 23 149.42 | 1044 | 37 320.37 | 2.27 | 2.72 | 64.96 | 66.84 | 5.81 | 23 719.33 |
| 1045 | 37 333.38 | 2.41 | 2.51 | 67.66 | 60.99 | 5.84 | 23 297.57 | 1046 | 37 339.23 | 2.17 | 2.88 | 63.28 | 69.88 | 5.63 | 23 882.87 |
| 1047 | 37 346.15 | 2.33 | 2.59 | 66.67 | 62.61 | 6.05 | 23 105.52 | 1048 | 37 354.43 | 2.45 | 2.65 | 68.42 | 59.61 | 5.75 | 23 932.66 |
| 1049 | 37 361.94 | 2.20 | 2.70 | 63.20 | 69.92 | 5.89 | 23 614.91 | 1050 | 37 376.10 | 2.30 | 2.67 | 62.99 | 70.39 | 5.66 | 23 960.46 |
| 1051 | 37 391.78 | 2.35 | 2.62 | 65.91 | 64.02 | 5.79 | 23 486.45 | 1052 | 37 394.03 | 2.44 | 2.62 | 68.83 | 59.06 | 5.79 | 23 748.11 |
| 1053 | 37 401.32 | 2.38 | 2.58 | 67.19 | 62.56 | 5.77 | 23 938.02 | 1054 | 37 418.34 | 2.44 | 2.48 | 68.74 | 58.94 | 5.82 | 23 363.40 |
| 1055 | 37 419.78 | 2.48 | 2.50 | 69.67 | 57.09 | 5.98 | 23 513.16 | 1056 | 37 426.18 | 2.36 | 2.51 | 68.79 | 59.16 | 5.92 | 22 961.64 |
| 1057 | 37 431.53 | 2.20 | 2.76 | 63.57 | 68.96 | 5.87 | 23 296.88 | 1058 | 37 448.88 | 2.33 | 2.62 | 66.85 | 62.93 | 5.85 | 23 796.67 |
| 1059 | 37 456.34 | 2.23 | 2.71 | 64.88 | 66.90 | 5.98 | 23 484.61 | 1060 | 37 466.67 | 2.32 | 2.69 | 65.73 | 65.31 | 5.77 | 23 820.00 |
| 1061 | 37 470.76 | 2.75 | 2.22 | 74.11 | 46.90 | 6.10 | 23 389.15 | 1062 | 37 479.08 | 2.61 | 2.39 | 70.86 | 54.49 | 5.95 | 23 665.72 |
| 1063 | 37 486.49 | 2.39 | 2.60 | 68.10 | 60.95 | 5.96 | 23 280.66 | 1064 | 37 500.48 | 2.42 | 2.49 | 68.79 | 58.05 | 5.99 | 23 331.97 |
| 1065 | 37 504.37 | 2.26 | 2.65 | 65.02 | 66.72 | 5.72 | 23 306.66 | 1066 | 37 523.09 | 2.28 | 2.77 | 65.70 | 65.64 | 5.73 | 23 880.64 |
| 1067 | 37 528.64 | 2.35 | 2.64 | 66.14 | 64.37 | 5.74 | 23 563.78 | 1068 | 37 533.47 | 2.27 | 2.63 | 65.64 | 64.59 | 6.01 | 23 100.80 |
| 1069 | 37 545.24 | 2.42 | 2.52 | 68.58 | 59.08 | 5.96 | 23 162.09 | 1070 | 37 549.95 | 2.31 | 2.61 | 65.55 | 64.32 | 5.97 | 23 449.32 |
| 1071 | 37 564.57 | 2.25 | 2.65 | 64.14 | 67.73 | 5.94 | 23 478.74 | 1072 | 37 567.65 | 2.33 | 2.66 | 66.61 | 63.67 | 5.81 | 23 641.98 |
| 1073 | 37 573.75 | 2.32 | 2.74 | 65.73 | 65.09 | 5.73 | 23 922.61 | 1074 | 37 578.36 | 2.25 | 2.72 | 64.66 | 68.07 | 5.80 | 23 626.59 |
| 1075 | 37 591.09 | 2.11 | 2.85 | 63.12 | 70.52 | 5.91 | 23 390.22 | 1076 | 37 600.15 | 2.34 | 2.78 | 62.99 | 70.41 | 5.54 | 24 716.76 |
| 1077 | 37 609.76 | 2.29 | 2.62 | 66.04 | 63.77 | 6.02 | 23 249.53 | 1078 | 37 620.11 | 2.35 | 2.63 | 67.18 | 62.33 | 5.79 | 23 614.16 |
| 1079 | 37 626.44 | 2.37 | 2.63 | 67.27 | 62.88 | 5.75 | 23 912.82 | 1080 | 37 639.68 | 2.54 | 2.43 | 70.37 | 55.56 | 5.80 | 23 537.96 |
| 1081 | 37 651.28 | 2.81 | 2.41 | 70.63 | 54.48 | 5.51 | 25 131.79 | 1082 | 37 660.74 | 2.35 | 2.69 | 66.25 | 65.00 | 5.64 | 23 932.89 |
| 1083 | 37 672.28 | 2.36 | 2.61 | 66.77 | 62.68 | 5.89 | 23 714.50 | 1084 | 37 675.87 | 2.59 | 2.43 | 71.48 | 53.81 | 5.75 | 23 980.11 |
| 1085 | 37 679.43 | 2.27 | 2.69 | 65.16 | 66.66 | 5.75 | 23 708.18 | 1086 | 37 689.61 | 2.31 | 2.68 | 67.10 | 63.09 | 5.88 | 23 533.07 |
| 1087 | 37 693.25 | 2.23 | 2.65 | 64.11 | 67.46 | 5.91 | 23 555.33 | 1088 | 37 714.61 | 2.55 | 2.50 | 68.83 | 59.22 | 5.80 | 24 269.02 |
| 1089 | 37 717.68 | 2.31 | 2.56 | 66.58 | 63.52 | 5.80 | 22 794.09 | 1090 | 37 723.69 | 2.43 | 2.60 | 67.44 | 61.58 | 5.81 | 23 759.69 |
| 1091 | 37 731.17 | 2.26 | 2.88 | 64.15 | 69.23 | 5.50 | 24 508.69 | 1092 | 37 734.10 | 2.49 | 2.54 | 69.91 | 57.73 | 5.85 | 23 616.41 |
| 1093 | 37 740.05 | 2.27 | 2.71 | 65.39 | 66.08 | 5.79 | 23 447.09 | 1094 | 37 757.70 | 2.25 | 2.76 | 64.23 | 68.74 | 5.58 | 23 764.79 |
| 1095 | 37 762.94 | 2.36 | 2.70 | 65.06 | 67.61 | 5.56 | 24 338.49 | 1096 | 37 766.62 | 2.41 | 2.59 | 68.92 | 59.41 | 5.88 | 23 779.82 |

(*continued*)

Table 2. Continued.

| $n$ | $E$ | $\langle R\rangle$ | $\langle r\rangle$ | $\langle\beta\rangle$ | $\langle\gamma\rangle$ | $C$ | $\langle V\rangle$ | $n$ | $E$ | $\langle R\rangle$ | $\langle r\rangle$ | $\langle\beta\rangle$ | $\langle\gamma\rangle$ | $C$ | $\langle V\rangle$ |
|---|---|---|---|---|---|---|---|---|---|---|---|---|---|---|---|
| 1097 | 37 774.64 | 2.08 | 2.95 | 60.82 | 74.59 | 5.58 | 23 903.51 | 1098 | 37 788.78 | 2.40 | 2.56 | 66.87 | 62.28 | 5.89 | 23 288.01 |
| 1099 | 37 795.94 | 2.41 | 2.61 | 67.80 | 60.88 | 5.69 | 23 839.21 | 1100 | 37 804.63 | 2.44 | 2.69 | 67.22 | 62.09 | 5.63 | 24 103.85 |
| 1101 | 37 808.41 | 2.38 | 2.68 | 67.46 | 61.18 | 5.86 | 23 864.68 | 1102 | 37 817.75 | 2.50 | 2.51 | 68.22 | 60.10 | 5.73 | 23 718.02 |
| 1103 | 37 818.66 | 2.45 | 2.56 | 68.39 | 59.57 | 5.77 | 23 479.48 | 1104 | 37 828.46 | 2.37 | 2.58 | 67.48 | 61.80 | 5.98 | 23 280.60 |
| 1105 | 37 836.84 | 2.51 | 2.48 | 69.34 | 57.43 | 5.84 | 23 700.83 | 1106 | 37 852.45 | 2.12 | 2.85 | 61.99 | 72.32 | 5.83 | 23 493.95 |
| 1107 | 37 861.48 | 2.39 | 2.62 | 66.42 | 63.69 | 5.67 | 23 901.40 | 1108 | 37 876.54 | 2.58 | 2.56 | 69.79 | 56.73 | 5.78 | 24 259.36 |
| 1109 | 37 883.71 | 2.38 | 2.65 | 67.71 | 62.15 | 5.70 | 23 777.11 | 1110 | 37 886.68 | 2.34 | 2.80 | 65.58 | 64.72 | 5.67 | 24 304.69 |
| 1111 | 37 893.61 | 2.45 | 2.63 | 67.83 | 60.91 | 5.69 | 24 021.02 | 1112 | 37 904.10 | 2.60 | 2.63 | 66.85 | 62.35 | 5.41 | 25 216.62 |
| 1113 | 37 919.21 | 2.18 | 2.83 | 62.54 | 70.20 | 5.99 | 23 664.41 | 1114 | 37 929.84 | 2.37 | 2.65 | 66.92 | 63.23 | 5.86 | 23 959.03 |
| 1115 | 37 938.38 | 2.21 | 2.75 | 63.27 | 69.46 | 5.87 | 23 695.20 | 1116 | 37 941.19 | 2.40 | 2.84 | 67.42 | 62.60 | 5.65 | 24 676.81 |
| 1117 | 37 945.58 | 2.24 | 2.73 | 64.18 | 68.39 | 5.65 | 23 839.96 | 1118 | 37 955.21 | 2.26 | 2.95 | 62.76 | 70.64 | 5.50 | 24 934.72 |
| 1119 | 37 959.10 | 2.82 | 2.38 | 70.82 | 53.64 | 5.55 | 24 797.26 | 1120 | 37 964.46 | 2.54 | 2.47 | 70.51 | 55.47 | 5.88 | 24 128.45 |
| 1121 | 37 976.20 | 2.48 | 2.57 | 68.07 | 60.38 | 5.76 | 24 290.21 | 1122 | 37 978.44 | 2.50 | 2.55 | 67.01 | 61.42 | 5.88 | 24 425.45 |
| 1123 | 37 990.90 | 2.42 | 2.60 | 65.69 | 64.50 | 5.66 | 24 160.24 | 1124 | 38 000.05 | 2.29 | 3.00 | 63.20 | 69.51 | 5.50 | 25 096.08 |
| 1125 | 38 005.28 | 2.47 | 2.65 | 65.21 | 66.38 | 5.43 | 24 584.74 | 1126 | 38 009.77 | 2.28 | 2.78 | 64.58 | 67.99 | 5.62 | 24 225.38 |
| 1127 | 38 024.74 | 2.37 | 2.58 | 67.11 | 61.34 | 5.89 | 23 375.73 | 1128 | 38 031.50 | 2.41 | 2.58 | 68.00 | 60.43 | 5.82 | 23 972.91 |
| 1129 | 38 039.62 | 2.43 | 2.59 | 67.81 | 60.66 | 5.84 | 23 751.44 | 1130 | 38 046.65 | 2.43 | 2.56 | 67.84 | 60.72 | 5.75 | 23 615.15 |
| 1131 | 38 068.24 | 2.35 | 2.72 | 65.68 | 64.24 | 5.86 | 23 952.36 | 1132 | 38 077.11 | 2.50 | 2.41 | 69.42 | 57.35 | 5.76 | 22 996.16 |
| 1133 | 38 084.75 | 2.36 | 2.61 | 66.68 | 63.20 | 5.79 | 23 633.29 | 1134 | 38 095.93 | 2.60 | 2.42 | 71.04 | 54.02 | 5.90 | 23 723.71 |
| 1135 | 38 099.17 | 2.26 | 2.78 | 64.86 | 68.10 | 5.54 | 23 908.98 | 1136 | 38 107.23 | 2.37 | 2.81 | 65.40 | 65.61 | 5.59 | 24 646.77 |
| 1137 | 38 115.41 | 2.35 | 2.71 | 66.71 | 63.05 | 5.83 | 23 893.00 | 1138 | 38 124.37 | 2.64 | 2.46 | 68.77 | 57.99 | 5.62 | 24 246.72 |
| 1139 | 38 125.45 | 2.34 | 2.82 | 64.43 | 67.86 | 5.50 | 24 613.82 | 1140 | 38 134.63 | 2.38 | 2.91 | 63.16 | 70.01 | 5.33 | 25 105.98 |
| 1141 | 38 143.46 | 2.34 | 2.61 | 65.06 | 65.15 | 5.94 | 23 803.12 | 1142 | 38 153.05 | 2.36 | 2.55 | 66.89 | 61.72 | 5.89 | 23 085.43 |
| 1143 | 38 158.61 | 2.21 | 2.87 | 62.16 | 72.10 | 5.55 | 24 347.03 | 1144 | 38 167.98 | 2.58 | 2.71 | 66.02 | 65.48 | 5.27 | 25 678.29 |
| 1145 | 38 181.11 | 2.39 | 2.69 | 66.71 | 62.74 | 5.67 | 24 374.54 | 1146 | 38 195.98 | 2.47 | 2.77 | 66.22 | 65.00 | 5.47 | 25 122.62 |
| 1147 | 38 199.98 | 2.44 | 2.58 | 67.63 | 60.63 | 5.76 | 23 714.35 | 1148 | 38 200.82 | 2.74 | 2.38 | 71.82 | 52.55 | 5.56 | 24 803.36 |
| 1149 | 38 212.20 | 2.69 | 2.64 | 68.03 | 60.26 | 5.43 | 25 274.26 | 1150 | 38 216.41 | 2.41 | 2.75 | 63.31 | 69.54 | 5.46 | 24 764.79 |
| 1151 | 38 226.10 | 2.57 | 2.43 | 69.36 | 57.65 | 5.88 | 23 861.54 | 1152 | 38 231.89 | 2.67 | 2.59 | 68.90 | 59.74 | 5.29 | 25 269.86 |
| 1153 | 38 242.04 | 2.12 | 2.87 | 60.30 | 75.30 | 5.64 | 23 948.97 | 1154 | 38 246.43 | 2.39 | 3.02 | 64.75 | 67.95 | 5.28 | 25 561.11 |
| 1155 | 38 252.69 | 2.42 | 2.73 | 67.21 | 63.07 | 5.64 | 24 789.22 | 1156 | 38 259.87 | 2.35 | 2.99 | 62.33 | 73.00 | 5.21 | 25 363.38 |
| 1157 | 38 270.73 | 2.65 | 2.46 | 69.39 | 57.90 | 5.63 | 24 553.12 | 1158 | 38 279.40 | 2.52 | 2.60 | 68.37 | 60.17 | 5.58 | 24 528.74 |
| 1159 | 38 283.18 | 2.63 | 2.38 | 71.18 | 53.66 | 5.78 | 23 848.92 | 1160 | 38 289.95 | 2.56 | 2.55 | 67.79 | 61.87 | 5.48 | 24 941.76 |
| 1161 | 38 296.76 | 2.40 | 2.63 | 65.94 | 64.25 | 5.58 | 24 332.30 | 1162 | 38 302.42 | 2.40 | 2.76 | 66.58 | 63.48 | 5.57 | 24 553.51 |
| 1163 | 38 307.51 | 2.22 | 2.91 | 62.60 | 71.51 | 5.51 | 24 434.11 | 1164 | 38 314.13 | 2.59 | 2.66 | 68.34 | 60.33 | 5.55 | 25 044.74 |
| 1165 | 38 328.41 | 2.33 | 2.76 | 65.23 | 66.07 | 5.74 | 24 282.89 | 1166 | 38 332.16 | 2.53 | 2.52 | 68.03 | 59.34 | 5.84 | 24 217.42 |
| 1167 | 38 345.12 | 2.64 | 2.48 | 69.36 | 57.44 | 5.67 | 24 332.11 | 1168 | 38 353.41 | 2.45 | 2.80 | 66.60 | 64.31 | 5.44 | 25 327.40 |
| 1169 | 38 357.40 | 2.57 | 2.65 | 69.73 | 57.65 | 5.70 | 24 547.86 | 1170 | 38 362.18 | 2.71 | 2.56 | 67.06 | 63.29 | 5.32 | 25 329.83 |
| 1171 | 38 377.41 | 2.33 | 2.75 | 63.38 | 69.30 | 5.60 | 24 476.74 | 1172 | 38 383.24 | 2.42 | 2.89 | 65.80 | 66.22 | 5.23 | 25 097.62 |
| 1173 | 38 390.05 | 2.63 | 2.65 | 70.38 | 55.99 | 5.44 | 25 187.57 | 1174 | 38 398.75 | 2.59 | 2.86 | 66.96 | 63.09 | 5.35 | 25 652.46 |
| 1175 | 38 404.84 | 2.54 | 2.62 | 68.81 | 59.55 | 5.47 | 24 623.44 | 1176 | 38 414.56 | 2.23 | 2.94 | 60.83 | 74.73 | 5.51 | 24 606.25 |
| 1177 | 38 423.53 | 2.72 | 2.88 | 65.83 | 65.72 | 4.93 | 26 402.34 | 1178 | 38 432.65 | 2.55 | 2.62 | 65.79 | 64.97 | 5.39 | 25 331.12 |
| 1179 | 38 442.55 | 2.36 | 3.33 | 63.11 | 71.62 | 4.91 | 26 437.55 | 1180 | 38 453.76 | 2.75 | 2.58 | 69.31 | 59.69 | 5.20 | 25 710.07 |
| 1181 | 38 455.90 | 3.00 | 2.65 | 67.94 | 61.10 | 4.94 | 26 463.06 | 1182 | 38 474.41 | 2.53 | 2.56 | 68.30 | 59.81 | 5.70 | 24 311.57 |
| 1183 | 38 477.06 | 3.78 | 2.08 | 75.84 | 45.26 | 4.46 | 28 608.72 | 1184 | 38 490.37 | 2.33 | 2.77 | 65.20 | 66.59 | 5.67 | 24 355.98 |
| 1185 | 38 500.31 | 2.88 | 2.46 | 71.72 | 52.62 | 5.49 | 25 053.40 | 1186 | 38 502.57 | 2.71 | 2.72 | 67.58 | 62.14 | 5.24 | 25 519.50 |
| 1187 | 38 509.54 | 3.85 | 2.38 | 70.07 | 57.62 | 4.36 | 28 538.70 | 1188 | 38 515.71 | 2.55 | 2.89 | 65.13 | 66.54 | 5.22 | 25 673.88 |
| 1189 | 38 522.17 | 2.86 | 2.61 | 69.99 | 57.37 | 5.18 | 26 029.17 | 1190 | 38 525.52 | 2.41 | 2.72 | 65.38 | 66.04 | 5.55 | 24 565.13 |
| 1191 | 38 541.32 | 2.50 | 2.81 | 67.14 | 63.50 | 5.45 | 25 072.30 | 1192 | 38 547.08 | 2.38 | 2.82 | 65.53 | 64.98 | 5.54 | 24 728.34 |
| 1193 | 38 553.79 | 2.70 | 2.73 | 69.02 | 59.21 | 5.39 | 25 387.13 | 1194 | 38 557.44 | 2.68 | 2.98 | 68.17 | 61.11 | 5.06 | 26 426.46 |
| 1195 | 38 568.62 | 2.63 | 2.87 | 67.14 | 63.73 | 5.16 | 26 163.17 | 1196 | 38 571.35 | 2.71 | 3.17 | 63.31 | 70.84 | 4.83 | 26 601.80 |
| 1197 | 38 578.26 | 3.17 | 2.55 | 67.84 | 62.12 | 5.00 | 26 131.52 | 1198 | 38 582.38 | 3.17 | 2.39 | 71.89 | 53.23 | 5.33 | 25 963.56 |
| 1199 | 38 588.10 | 3.60 | 2.54 | 70.08 | 57.27 | 4.68 | 27 342.11 | 1200 | 38 596.62 | 2.43 | 2.70 | 65.58 | 65.49 | 5.53 | 24 670.43 |
| 1201 | 38 598.07 | 2.83 | 2.93 | 65.80 | 66.57 | 4.96 | 26 045.55 | 1202 | 38 610.92 | 3.14 | 2.63 | 69.53 | 57.78 | 5.20 | 26 047.78 |
| 1203 | 38 619.78 | 2.35 | 3.16 | 63.30 | 70.80 | 5.17 | 25 793.78 | 1204 | 38 623.80 | 4.73 | 2.42 | 73.44 | 51.16 | 4.14 | 28 822.61 |
| 1205 | 38 632.90 | 3.88 | 2.58 | 69.57 | 59.18 | 4.58 | 27 479.89 | 1206 | 38 633.91 | 2.35 | 2.95 | 61.90 | 73.61 | 5.28 | 25 118.52 |
| 1207 | 38 640.22 | 4.80 | 2.43 | 72.37 | 53.50 | 4.33 | 28 209.45 | 1208 | 38 649.78 | 6.51 | 2.40 | 73.92 | 51.52 | 3.54 | 30 366.94 |
| 1209 | 38 655.45 | 6.88 | 2.35 | 72.92 | 53.82 | 3.58 | 29 850.34 | | | | | | | | |

Table 3. Energy levels of $B_1$ symmetry for $D_2H^+$. Units are $cm^{-1}$ for $E$, $C$ and $V$, $a_0$ for $r$ and $R$, degrees for $\beta$ and $\gamma$.

| $n$ | $E$ | $\langle R\rangle$ | $\langle r\rangle$ | $\langle\beta\rangle$ | $\langle\gamma\rangle$ | $C$ | $\langle V\rangle$ | $n$ | $E$ | $\langle R\rangle$ | $\langle r\rangle$ | $\langle\beta\rangle$ | $\langle\gamma\rangle$ | $C$ | $\langle V\rangle$ |
|---|---|---|---|---|---|---|---|---|---|---|---|---|---|---|---|
| 1 | 5640.74 | 1.56 | 1.70 | 62.60 | 56.72 | 12.49 | 2953.82 | 2 | 7622.49 | 1.54 | 1.78 | 61.14 | 60.37 | 11.88 | 4006.11 |
| 3 | 8237.79 | 1.64 | 1.71 | 63.58 | 55.28 | 12.10 | 4422.24 | 4 | 9394.66 | 1.64 | 1.75 | 64.07 | 55.86 | 11.54 | 5131.94 |
| 37 | 16 786.00 | 1.65 | 2.04 | 60.97 | 65.83 | 9.62 | 9695.39 | 38 | 16 939.90 | 1.76 | 1.94 | 65.03 | 58.89 | 9.76 | 10 038.75 |
| 181 | 25 011.63 | 1.96 | 2.15 | 66.44 | 59.89 | 8.12 | 15 280.12 | 182 | 25 040.76 | 2.06 | 2.07 | 69.42 | 55.45 | 8.03 | 15 340.59 |
| 439 | 31 191.95 | 2.14 | 2.37 | 67.03 | 61.34 | 6.94 | 19 357.70 | 440 | 31 204.66 | 2.18 | 2.32 | 67.70 | 59.58 | 6.96 | 19 196.46 |
| 915 | 37 183.70 | 2.34 | 2.70 | 66.27 | 63.93 | 5.70 | 23 861.26 | 916 | 37 195.35 | 2.18 | 2.75 | 64.23 | 68.87 | 5.85 | 23 485.29 |
| 917 | 37 203.48 | 2.37 | 2.61 | 68.24 | 60.06 | 5.84 | 23 718.36 | 918 | 37 230.35 | 2.32 | 2.68 | 66.24 | 65.65 | 5.65 | 23 823.46 |
| 919 | 37 246.24 | 2.37 | 2.63 | 68.56 | 58.90 | 6.05 | 23 421.46 | 920 | 37 246.91 | 2.36 | 2.60 | 67.98 | 61.14 | 5.93 | 23 446.84 |
| 921 | 37 261.01 | 2.47 | 2.50 | 69.40 | 58.20 | 5.83 | 23 619.06 | 922 | 37 268.86 | 2.40 | 2.55 | 68.48 | 60.35 | 5.85 | 23 461.00 |
| 923 | 37 273.72 | 2.46 | 2.60 | 69.20 | 58.33 | 5.64 | 24 074.85 | 924 | 37 283.75 | 2.16 | 2.75 | 63.29 | 69.79 | 5.75 | 23 255.35 |
| 925 | 37 303.89 | 2.40 | 2.50 | 68.93 | 58.08 | 6.04 | 23 260.00 | 926 | 37 308.56 | 2.30 | 2.64 | 66.48 | 63.76 | 5.89 | 23 256.04 |
| 927 | 37 317.25 | 2.40 | 2.71 | 67.83 | 62.46 | 5.56 | 24 386.23 | 928 | 37 329.58 | 2.19 | 2.71 | 63.44 | 68.97 | 5.79 | 23 269.42 |
| 929 | 37 338.35 | 2.38 | 2.60 | 67.51 | 60.70 | 5.87 | 23 752.24 | 930 | 37 347.25 | 2.49 | 2.54 | 67.20 | 61.99 | 5.62 | 24 258.37 |
| 931 | 37 358.67 | 2.36 | 2.62 | 68.29 | 60.32 | 5.85 | 23 549.85 | 932 | 37 361.54 | 2.43 | 2.53 | 68.48 | 59.42 | 5.89 | 23 518.53 |
| 933 | 37 371.28 | 2.27 | 2.71 | 66.46 | 63.41 | 5.77 | 23 804.85 | 934 | 37 392.33 | 2.36 | 2.58 | 66.33 | 63.12 | 5.73 | 23 540.72 |
| 935 | 37 396.73 | 2.36 | 2.68 | 67.54 | 62.12 | 5.75 | 23 930.64 | 936 | 37 408.43 | 2.35 | 2.56 | 67.12 | 61.35 | 5.97 | 23 322.10 |
| 937 | 37 413.54 | 2.45 | 2.48 | 68.77 | 58.49 | 5.73 | 23 522.74 | 938 | 37 426.23 | 2.53 | 2.48 | 69.85 | 56.62 | 5.81 | 23 452.86 |
| 939 | 37 433.92 | 2.31 | 2.59 | 66.71 | 63.71 | 5.85 | 23 323.51 | 940 | 37 439.21 | 2.47 | 2.52 | 69.42 | 58.16 | 5.75 | 23 891.64 |
| 941 | 37 456.91 | 2.43 | 2.61 | 68.91 | 59.98 | 5.75 | 24 042.70 | 942 | 37 467.36 | 2.20 | 2.75 | 64.42 | 68.11 | 5.84 | 23 467.00 |
| 943 | 37 478.41 | 2.13 | 2.81 | 62.04 | 72.45 | 5.72 | 23 418.25 | 944 | 37 482.56 | 2.38 | 2.66 | 67.20 | 62.60 | 5.74 | 23 825.03 |
| 945 | 37 489.39 | 2.37 | 2.70 | 67.19 | 63.60 | 5.60 | 24 067.10 | 946 | 37 502.05 | 2.30 | 2.73 | 64.05 | 68.69 | 5.60 | 24 191.35 |
| 947 | 37 511.85 | 2.50 | 2.45 | 70.49 | 54.65 | 5.98 | 23 295.09 | 948 | 37 524.30 | 2.25 | 2.80 | 64.51 | 67.61 | 5.69 | 23 624.33 |
| 949 | 37 538.52 | 2.24 | 2.74 | 65.18 | 66.33 | 5.78 | 23 572.15 | 950 | 37 542.38 | 2.36 | 2.66 | 67.81 | 61.68 | 5.79 | 23 721.84 |
| 951 | 37 544.33 | 2.35 | 2.61 | 67.41 | 62.40 | 5.81 | 23 468.55 | 952 | 37 550.05 | 2.42 | 2.62 | 67.49 | 61.65 | 5.79 | 24 125.50 |
| 953 | 37 564.77 | 2.38 | 2.66 | 69.01 | 59.29 | 5.90 | 23 760.81 | 954 | 37 571.00 | 2.30 | 2.70 | 65.90 | 64.14 | 5.75 | 23 410.90 |
| 955 | 37 577.65 | 2.41 | 2.62 | 68.21 | 60.64 | 5.80 | 23 614.59 | 956 | 37 591.88 | 2.56 | 2.49 | 69.51 | 57.67 | 5.67 | 24 121.93 |
| 957 | 37 599.20 | 2.30 | 2.73 | 64.45 | 67.56 | 5.66 | 24 088.50 | 958 | 37 620.93 | 2.30 | 2.79 | 65.11 | 67.45 | 5.55 | 24 253.90 |
| 959 | 37 627.93 | 2.23 | 2.75 | 64.36 | 68.69 | 5.60 | 23 936.13 | 960 | 37 645.47 | 2.44 | 2.60 | 68.07 | 60.30 | 5.66 | 23 845.48 |
| 961 | 37 651.64 | 2.40 | 2.61 | 68.50 | 60.48 | 5.89 | 23 394.86 | 962 | 37 655.96 | 2.30 | 2.70 | 65.39 | 66.35 | 5.56 | 23 861.30 |
| 963 | 37 662.64 | 2.31 | 2.63 | 65.36 | 65.63 | 5.79 | 23 615.81 | 964 | 37 670.16 | 2.54 | 2.43 | 70.76 | 54.17 | 5.94 | 23 563.38 |
| 965 | 37 677.74 | 2.33 | 2.80 | 65.97 | 64.89 | 5.51 | 24 230.27 | 966 | 37 693.32 | 2.61 | 2.37 | 72.05 | 50.59 | 6.13 | 23 331.57 |
| 967 | 37 702.29 | 2.33 | 2.68 | 67.25 | 62.54 | 5.84 | 23 634.82 | 968 | 37 709.48 | 2.49 | 2.48 | 69.17 | 57.18 | 5.90 | 23 680.99 |
| 969 | 37 719.50 | 2.30 | 2.62 | 65.94 | 64.17 | 5.77 | 23 494.92 | 970 | 37 732.02 | 2.42 | 2.65 | 68.19 | 60.95 | 5.70 | 24 033.78 |
| 971 | 37 736.53 | 2.48 | 2.45 | 70.12 | 55.28 | 5.84 | 23 078.19 | 972 | 37 739.20 | 2.25 | 2.77 | 64.46 | 68.63 | 5.68 | 24 037.08 |
| 973 | 37 759.17 | 2.52 | 2.44 | 69.42 | 57.03 | 5.80 | 23 627.30 | 974 | 37 766.27 | 2.31 | 2.72 | 65.51 | 65.43 | 5.76 | 23 910.23 |
| 975 | 37 774.29 | 2.70 | 2.33 | 72.89 | 50.11 | 5.90 | 23 534.55 | 976 | 37 783.48 | 2.08 | 2.95 | 61.40 | 73.65 | 5.76 | 24 061.25 |
| 977 | 37 793.40 | 2.32 | 2.70 | 66.18 | 65.29 | 5.64 | 23 979.30 | 978 | 37 806.32 | 2.39 | 2.64 | 68.02 | 60.26 | 5.76 | 23 984.32 |
| 979 | 37 808.79 | 2.35 | 2.68 | 66.46 | 64.03 | 5.70 | 23 942.31 | 980 | 37 817.87 | 2.10 | 2.94 | 61.38 | 74.19 | 5.53 | 24 069.45 |
| 981 | 37 825.40 | 2.38 | 2.67 | 67.56 | 61.91 | 5.80 | 23 894.45 | 982 | 37 838.51 | 2.38 | 2.64 | 67.12 | 62.37 | 5.63 | 24 013.14 |
| 983 | 37 845.39 | 2.52 | 2.56 | 69.53 | 56.50 | 5.85 | 23 866.75 | 984 | 37 861.22 | 2.48 | 2.67 | 68.94 | 58.77 | 5.75 | 24 491.58 |
| 985 | 37 873.83 | 2.34 | 2.69 | 66.08 | 64.52 | 5.77 | 24 016.64 | 986 | 37 878.67 | 2.50 | 2.57 | 69.71 | 56.93 | 5.77 | 23 893.89 |
| 987 | 37 886.50 | 2.21 | 2.80 | 63.28 | 70.15 | 5.70 | 24 042.20 | 988 | 37 891.91 | 2.51 | 2.52 | 69.45 | 57.43 | 5.70 | 23 904.12 |
| 989 | 37 896.14 | 2.42 | 2.67 | 67.76 | 62.04 | 5.62 | 24 275.42 | 990 | 37 908.47 | 2.56 | 2.55 | 70.12 | 56.05 | 5.90 | 24 177.04 |
| 991 | 37 922.43 | 2.24 | 2.79 | 63.85 | 68.68 | 5.71 | 23 982.75 | 992 | 37 935.47 | 2.29 | 2.91 | 64.20 | 68.39 | 5.49 | 24 576.50 |
| 993 | 37 937.39 | 2.25 | 2.78 | 64.51 | 67.87 | 5.74 | 23 847.06 | 994 | 37 945.33 | 2.44 | 2.67 | 67.02 | 63.34 | 5.53 | 24 613.62 |
| 995 | 37 950.33 | 2.46 | 2.59 | 67.82 | 61.50 | 5.65 | 24 794.86 | 996 | 37 954.56 | 2.47 | 2.60 | 68.42 | 59.60 | 5.77 | 24 018.28 |
| 997 | 37 971.43 | 2.34 | 2.71 | 65.42 | 66.09 | 5.67 | 24 087.73 | 998 | 37 983.65 | 2.18 | 2.90 | 62.53 | 72.31 | 5.55 | 24 285.23 |
| 999 | 37 993.17 | 2.31 | 2.93 | 64.01 | 68.60 | 5.59 | 24 921.38 | 1000 | 37 996.51 | 2.46 | 2.59 | 68.58 | 59.78 | 5.69 | 23 871.45 |
| 1001 | 38 009.49 | 2.52 | 2.74 | 67.73 | 61.55 | 5.43 | 24 890.99 | 1002 | 38 010.54 | 2.47 | 2.64 | 67.77 | 62.09 | 5.56 | 24 368.66 |
| 1003 | 38 015.89 | 2.21 | 2.81 | 63.40 | 70.39 | 5.57 | 24 082.60 | 1004 | 38 040.18 | 2.57 | 2.58 | 69.03 | 58.59 | 5.63 | 24 488.47 |
| 1005 | 38 044.76 | 2.32 | 2.77 | 64.09 | 68.31 | 5.50 | 24 426.75 | 1006 | 38 059.31 | 2.55 | 2.45 | 70.06 | 56.23 | 5.64 | 23 773.87 |
| 1007 | 38 071.74 | 2.27 | 2.79 | 64.92 | 67.27 | 5.64 | 24 036.11 | 1008 | 38 079.68 | 2.65 | 2.38 | 71.63 | 52.45 | 5.72 | 23 383.57 |
| 1009 | 38 087.01 | 2.53 | 2.55 | 70.11 | 57.00 | 5.65 | 24 110.36 | 1010 | 38 092.43 | 2.35 | 2.68 | 66.83 | 63.70 | 5.66 | 23 971.79 |

(*continued*)

Table 3. Continued.

| $n$ | $E$ | $\langle R\rangle$ | $\langle r\rangle$ | $\langle\beta\rangle$ | $\langle\gamma\rangle$ | $C$ | $\langle V\rangle$ | $n$ | $E$ | $\langle R\rangle$ | $\langle r\rangle$ | $\langle\beta\rangle$ | $\langle\gamma\rangle$ | $C$ | $\langle V\rangle$ |
|---|---|---|---|---|---|---|---|---|---|---|---|---|---|---|---|
| 1011 | 38 094.86 | 2.64 | 2.75 | 67.62 | 61.45 | 5.25 | 25 750.85 | 1012 | 38 107.58 | 2.65 | 2.29 | 71.43 | 52.21 | 5.77 | 22 845.17 |
| 1013 | 38 109.91 | 2.40 | 2.74 | 64.36 | 67.89 | 5.59 | 25 061.36 | 1014 | 38 118.18 | 2.41 | 2.64 | 68.25 | 60.86 | 5.72 | 24 065.34 |
| 1015 | 38 131.30 | 2.58 | 2.54 | 71.00 | 54.61 | 5.73 | 24 056.67 | 1016 | 38 137.02 | 2.62 | 2.50 | 71.58 | 52.71 | 5.80 | 23 923.92 |
| 1017 | 38 153.75 | 2.49 | 2.62 | 67.51 | 61.66 | 5.59 | 24 534.39 | 1018 | 38 159.11 | 2.39 | 2.70 | 67.75 | 62.31 | 5.77 | 24 250.66 |
| 1019 | 38 169.20 | 2.48 | 2.66 | 66.97 | 63.19 | 5.50 | 24 819.79 | 1020 | 38 177.76 | 2.35 | 2.60 | 67.18 | 62.26 | 5.80 | 23 575.96 |
| 1021 | 38 186.93 | 2.18 | 3.27 | 60.27 | 75.41 | 5.15 | 25 520.67 | 1022 | 38 198.78 | 2.54 | 2.54 | 70.05 | 57.73 | 5.55 | 24 353.13 |
| 1023 | 38 215.29 | 2.35 | 2.72 | 66.67 | 63.58 | 5.68 | 24 203.45 | 1024 | 38 224.50 | 2.27 | 2.83 | 65.50 | 66.86 | 5.60 | 24 294.51 |
| 1025 | 38 234.40 | 2.63 | 2.81 | 68.53 | 60.00 | 5.44 | 25 356.80 | 1026 | 38 238.44 | 2.57 | 2.56 | 70.04 | 56.96 | 5.77 | 24 016.28 |
| 1027 | 38 243.72 | 2.28 | 2.94 | 63.56 | 70.35 | 5.34 | 24 743.82 | 1028 | 38 247.57 | 2.57 | 2.58 | 70.23 | 57.14 | 5.67 | 24 620.56 |
| 1029 | 38 253.23 | 2.54 | 2.63 | 66.94 | 62.66 | 5.54 | 24 559.35 | 1030 | 38 270.45 | 2.45 | 2.70 | 67.28 | 63.90 | 5.45 | 25 116.22 |
| 1031 | 38 273.57 | 2.65 | 2.65 | 70.46 | 55.68 | 5.50 | 24 791.36 | 1032 | 38 282.53 | 2.45 | 2.79 | 66.04 | 65.50 | 5.35 | 24 740.49 |
| 1033 | 38 292.64 | 2.46 | 2.78 | 65.83 | 64.62 | 5.54 | 25 188.11 | 1034 | 38 296.31 | 2.75 | 2.46 | 69.97 | 56.93 | 5.36 | 24 899.84 |
| 1035 | 38 301.15 | 2.35 | 2.66 | 66.86 | 64.19 | 5.68 | 24 030.53 | 1036 | 38 308.51 | 2.47 | 2.81 | 66.29 | 64.42 | 5.43 | 25 159.45 |
| 1037 | 38 322.43 | 2.56 | 2.59 | 69.95 | 56.69 | 5.81 | 24 271.02 | 1038 | 38 327.11 | 2.52 | 2.67 | 68.31 | 60.33 | 5.60 | 24 446.86 |
| 1039 | 38 336.65 | 2.94 | 2.55 | 71.38 | 54.90 | 5.20 | 26 278.11 | 1040 | 38 349.18 | 2.45 | 2.62 | 68.21 | 61.80 | 5.57 | 24 264.56 |
| 1041 | 38 350.91 | 2.52 | 2.67 | 67.87 | 61.11 | 5.47 | 25 159.75 | 1042 | 38 358.50 | 2.28 | 2.85 | 64.06 | 69.11 | 5.47 | 24 541.82 |
| 1043 | 38 373.61 | 2.79 | 2.36 | 75.46 | 45.04 | 5.95 | 24 343.41 | 1044 | 38 377.01 | 2.55 | 2.63 | 69.77 | 56.60 | 5.59 | 24 600.17 |
| 1045 | 38 381.70 | 2.26 | 2.82 | 65.19 | 66.60 | 5.65 | 24 319.70 | 1046 | 38 399.48 | 2.85 | 2.48 | 71.22 | 54.49 | 5.31 | 25 430.67 |
| 1047 | 38 407.86 | 2.57 | 2.78 | 66.68 | 63.90 | 5.31 | 25 425.53 | 1048 | 38 419.38 | 2.46 | 3.03 | 66.00 | 65.49 | 5.23 | 25 615.51 |
| 1049 | 38 422.76 | 2.41 | 2.66 | 67.73 | 62.28 | 5.52 | 24 504.47 | 1050 | 38 435.72 | 2.40 | 2.68 | 66.40 | 63.24 | 5.55 | 24 213.34 |
| 1051 | 38 443.28 | 2.63 | 2.87 | 68.13 | 60.60 | 5.24 | 26 123.34 | 1052 | 38 447.58 | 2.78 | 2.60 | 69.23 | 58.58 | 5.30 | 25 637.06 |
| 1053 | 38 451.67 | 2.49 | 2.56 | 68.46 | 61.17 | 5.61 | 24 290.03 | 1054 | 38 462.02 | 2.28 | 2.86 | 64.81 | 68.41 | 5.46 | 24 699.44 |
| 1055 | 38 472.67 | 2.42 | 2.65 | 67.65 | 62.05 | 5.59 | 24 492.90 | 1056 | 38 476.47 | 2.61 | 2.51 | 70.69 | 54.99 | 5.67 | 24 039.18 |
| 1057 | 38 483.11 | 2.39 | 2.81 | 66.19 | 64.70 | 5.53 | 24 952.42 | 1058 | 38 485.80 | 2.31 | 2.72 | 65.57 | 66.31 | 5.58 | 24 025.03 |
| 1059 | 38 497.23 | 2.39 | 3.09 | 65.22 | 67.65 | 5.23 | 25 247.23 | 1060 | 38 511.47 | 2.52 | 2.99 | 66.44 | 64.10 | 5.28 | 25 656.26 |
| 1061 | 38 514.74 | 3.31 | 2.55 | 72.93 | 51.85 | 4.73 | 27 853.90 | 1062 | 38 520.27 | 2.81 | 2.51 | 72.35 | 51.89 | 5.47 | 25 430.14 |
| 1063 | 38 525.74 | 2.49 | 2.84 | 65.81 | 65.91 | 5.31 | 25 473.81 | 1064 | 38 532.24 | 2.37 | 3.04 | 63.08 | 69.96 | 5.42 | 25 530.20 |
| 1065 | 38 548.31 | 3.07 | 2.67 | 72.82 | 52.05 | 4.85 | 26 969.61 | 1066 | 38 556.76 | 2.24 | 2.98 | 62.07 | 72.61 | 5.28 | 24 908.55 |
| 1067 | 38 566.38 | 2.47 | 2.88 | 66.70 | 64.38 | 5.37 | 25 188.84 | 1068 | 38 579.87 | 2.91 | 2.42 | 70.69 | 55.98 | 5.22 | 25 996.85 |
| 1069 | 38 583.00 | 2.36 | 2.91 | 64.78 | 67.92 | 5.40 | 24 914.41 | 1070 | 38 587.78 | 2.52 | 3.12 | 64.43 | 69.50 | 4.96 | 26 437.36 |
| 1071 | 38 590.30 | 2.53 | 3.05 | 63.70 | 70.30 | 4.96 | 26 357.06 | 1072 | 38 596.81 | 2.43 | 2.76 | 66.37 | 63.96 | 5.49 | 24 897.32 |
| 1073 | 38 616.36 | 2.60 | 2.78 | 67.58 | 62.08 | 5.30 | 25 500.54 | 1074 | 38 622.05 | 3.29 | 2.35 | 74.20 | 48.49 | 5.02 | 27 057.47 |
| 1075 | 38 628.54 | 2.99 | 2.47 | 70.82 | 55.89 | 5.21 | 25 585.60 | 1076 | 38 646.92 | 3.18 | 2.64 | 71.44 | 54.28 | 4.96 | 26 619.90 |
| 1077 | 38 652.81 | 2.68 | 2.60 | 68.33 | 60.96 | 5.43 | 24 979.71 | 1078 | 38 655.33 | 2.76 | 2.86 | 64.56 | 68.34 | 5.03 | 26 741.07 |

reflected in the mean inter-particle distance, which is much bigger in the higher energy states than in the lowest ones, leading to the idea of how the dissociation wavefunctions are elongated by nature. This property of near dissociation states can be highlighted by considering, besides the mean value of the various observables, also their root-mean-square deviation [25]. The latter is defined, if we consider the observable $x$, as $\Delta x = (\langle x^2\rangle - \langle x\rangle^2)^{1/2}$. For example, the ground state root-mean-square deviation of the inter-particle distance is of the order of $0.2a_0$, showing that the molecule is fairly stiff and the nuclei move only close to their average separation, which almost coincides with the minimum of the PES. Conversely, for the higher states this standard deviation is never smaller than $3a_0$. Such values are typical of a very extended wavefunction, as can be seen from figures 3 and 4.

Among the levels closest to dissociation, it is possible to recognize two different classes of states: a first set of states that have a compact geometry and which we will refer to as standard three-body states, and a second set of states called Asymptotic Vibrational States (AVS) that have been studied for $H_3^+$ previously [9]. The AVS have a strongly marked isosceles shape, where two particles are close to each other and form a diatom, and the third particle orbits around them at a large distance. This is reflected in the large value of the dissociative coordinate $R$ and the small value of $C$, as well as in the mean values of the angles D–H–D and H–D–D. The diatom structure is less pronounced in $H_3^+$ than $D_2H^+$, for reasons of symmetry.

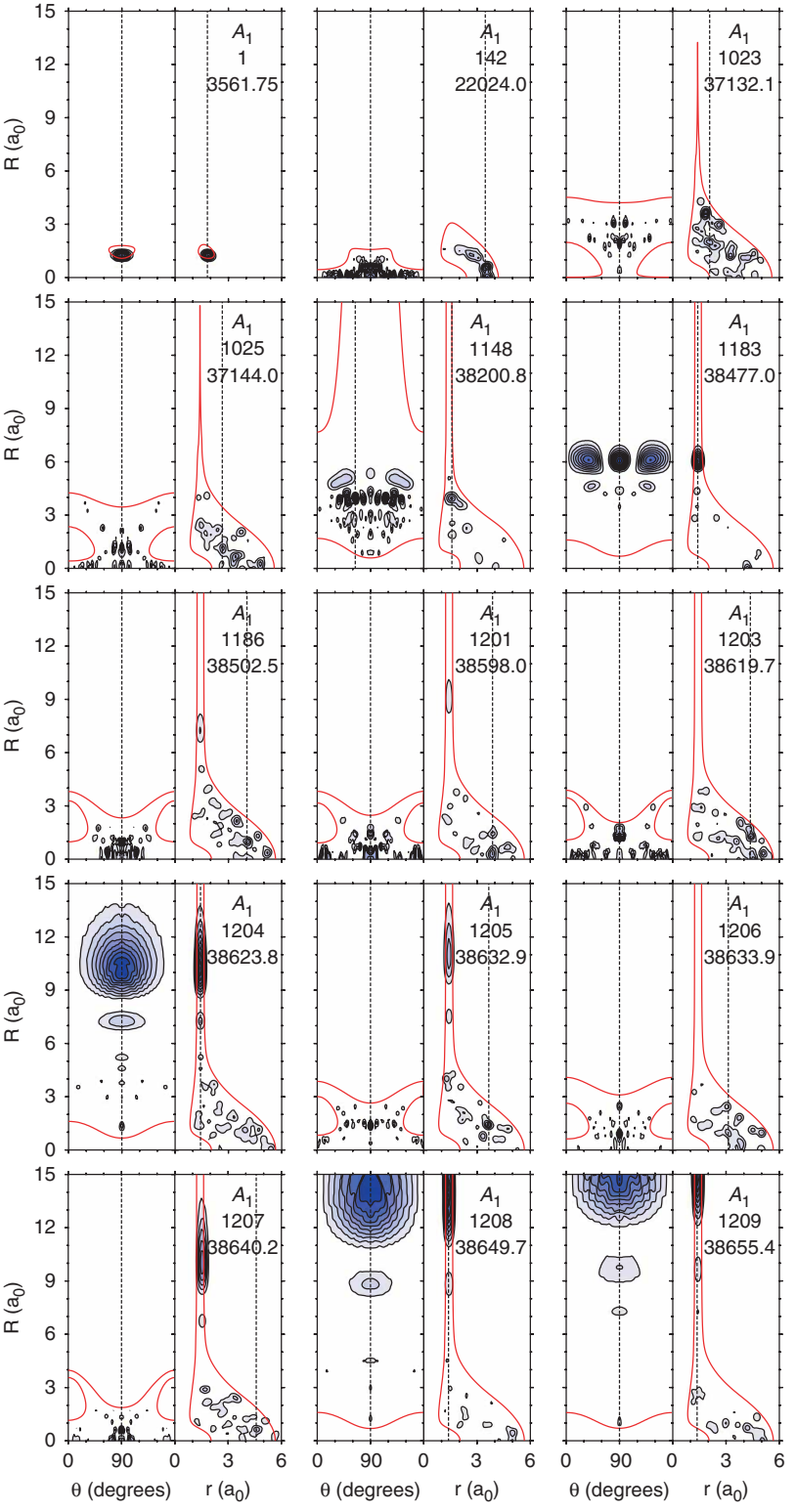


Figure 3. Two-dimensional slices through the molecular probability density $\psi^2$ for several $D_2H^+$ states of $A_1$ symmetry. The density is normalized so that $\int \psi^2 dr_1 dr_2 d\alpha = 1$, where $\{r_1, r_2, \alpha\}$ are the Radau coordinates. For the sake of clarity, however, the plots use Jacobi coordinates to parametrize the probability density. The left-hand part of the plot represents the cut $\psi(r_{\max}, R, \theta)^2$, whereas the right-hand part shows the cut $\psi(r, R, \theta_{\max})^2$. The probability is normalized so that $\Psi(r_{\max}, R_{\max}, \theta_{\max})^2 = 1$, where the point $\{r_{\max}, R_{\max}, \theta_{\max}\}$ is associated with the absolute maximum of the density, and the cuts are chosen so that this point is contained in both parts of the plot. Contours represent steps of 10% in probability. The continuum lines show the classical turning point.

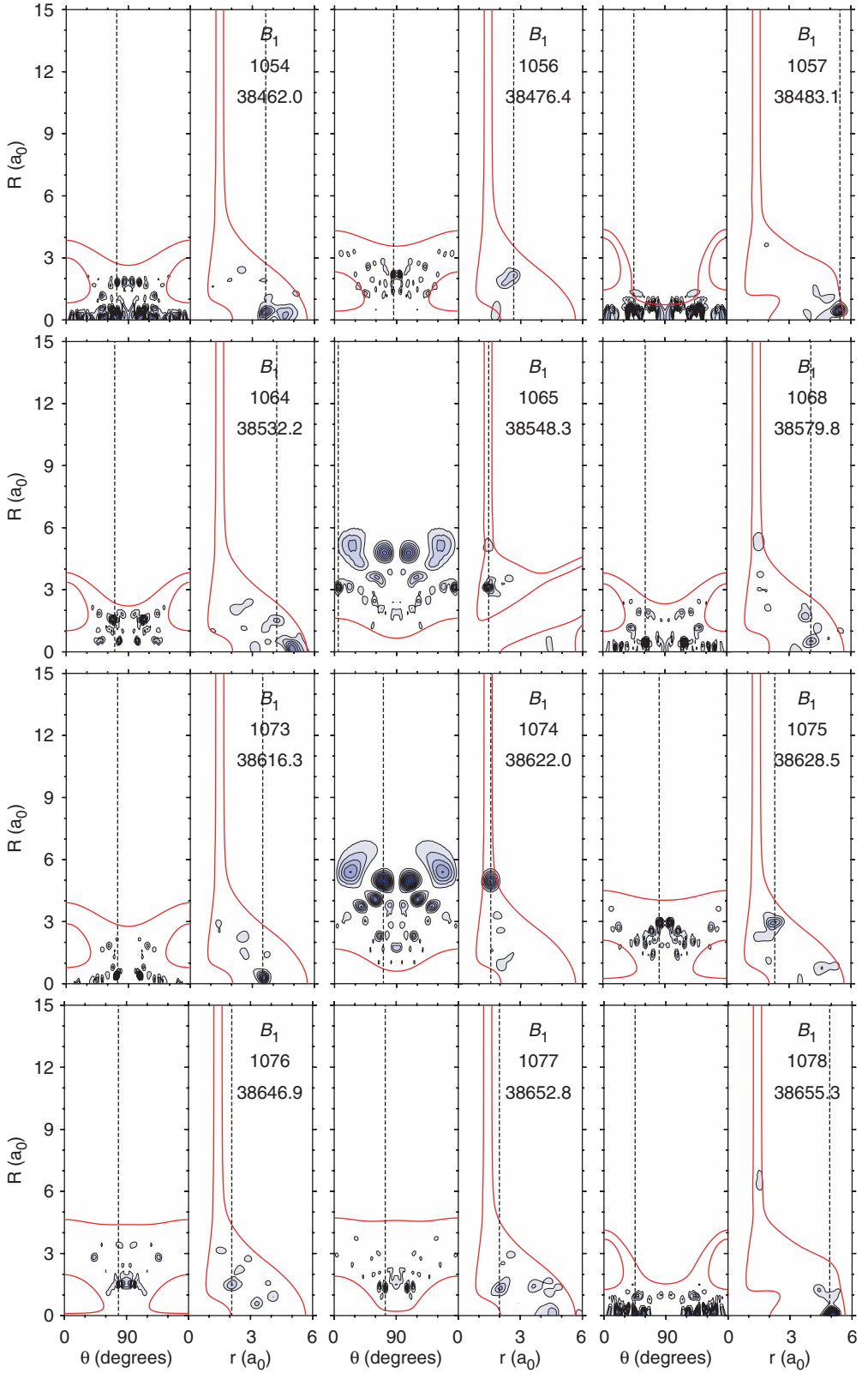


Figure 4. Two-dimensional slices through the molecular probability density $\psi^2$ for several $D_2H^+$ states of $B_1$ symmetry. For explanation of the plots, see the caption of figure 3.

Physically, one could interpret the AVS as weakly bound ion–diatom states, where the diatom behaves as if the third particle were a small perturbation, and the ion then is bound to the diatom due to the weak charge-induced dipole and charge quadrupole forces. However, in both molecules this interpretation is not completely satisfactory. In order to test the '2+1' interpretation of the AVS, one can compare the bond length $r$ of the diatom components with the equivalent distance in the free diatoms. Even for the states with the strongest AVS features, one finds that this distance is larger than in the corresponding diatom, where $\langle r \rangle$ is $1.448a_0$ for $H_2$ and $1.432a_0$ for $D_2$. Thus we must conclude that the AVS states presented in table 6 cannot be considered as pure '2+1' states, but rather as mixtures of '2+1' and standard three-body states. It is likely that the number of vibration band origins we have found is not exhaustive, and that if our study is extended to a larger range of the coordinates $r$, $R$ we will find more states for both molecules. We would then expect those states to show stronger '2+1' characteristics.

Figures 3 and 4 show the probability density for several states for $D_2H^+$ of $A_1$ and $B_1$ symmetry, respectively. These figures give two different cuts through the four-dimensional surface $|\psi(r, R, \theta)|^2$. These cuts are bound to be subjective and therefore different cuts could show other aspects of the problem. Nevertheless, a careful choice of cuts may provide some insight into the properties of the wavefunctions. The first graph in figure 3 shows the probability density for the ground state of $D_2H^+$, so as to have a clear visual perception of how compact this state is, compared with the high-lying ones. In the same figure, the next two graphs show two states (1023 $A_1$ and 1025 $A_1$) below $D_e$ but high in energy. Both show a very complex nodal structure in the intermediate region, possibly due to the requirement of orthogonality to the lower states. Among the higher-lying states, it is possible to recognize a number of AVS states of the $D_2$+H kind (1183 $A_1$, 1204 $A_1$, 1208 $A_1$ and 1209 $A_1$), similar to those found in $H_3^+$, as well as standard three-body states (1206 $A_1$) or mixtures (1205 $A_1$, 1207 $A_1$). It is also possible to recognize linear D–H–D configurations (1201 $A_1$, 1186 $A_1$ and 1203 $A_1$).

The $B_1$ states shown in figure 4 are also interesting. Despite the high energy of those levels, there are no AVS states of the $D_2$–H kind as in the other symmetry. This is due to the fact that the $D_2$ pair has the wrong (odd) inter-nuclear symmetry with respect to the ground vibrational $D_2$ state (which is even). This can be seen by comparing state 1074 $B_1$ in figure 4 with state 1204 $A_1$ in figure 3. On the other hand, the last state (1078 $B_1$) shows a clear DH–D character, where the two D nuclei are apart from each other and the H sits symmetrically on both of them.

## 4. Beyond the Born–Oppenheimer approximation

In our calculations for $D_2H^+$, we have neglected all effects beyond the non-relativistic BO framework. In a previous ultra-high-accuracy study [26], Polyansky and Tennyson discussed the importance of some of the corrections to the non-relativistic BO approximation. Their work was limited to vibrational band origins below $10\,000\,\mathrm{cm}^{-1}$. The relativistic and adiabatic BO corrections to the $1^1A'$ PES are reported in [26] as polynomial surfaces, whose coefficients are fitted to calculated data points. Unfortunately, those surfaces are accurate in a range which is much smaller than the extent of the high-lying bound states of $D_2H^+$, and therefore it is not meaningful to evaluate their effect on the calculated states. However, Polyansky and Tennyson concluded that the effect on the lowest states of the relativistic effect is very small and the adiabatic correction is of the order of $1\,\mathrm{cm}^{-1}$. There is no reason to believe that these will be of a different order of magnitude for the higher energy states.

The study of off-diagonal BO or non-adiabatic corrections is particularly demanding as it involves the calculation of all the PESs, their derivatives with respect to the nuclear coordinates, and the coupling between them. It is very difficult, even for systems as small as triatomics, to even evaluate these corrections approximately for low-lying states [27], and one generally has to resort to simple models instead.

It has been shown in previous works that those very complicated effects can be modeled effectively by allowing for the nuclear masses to be varied. This procedure is known as mass scaling and was first introduced by Bunker and Moss for diatomics [28]. Subsequently, Polyansky and Tennyson applied the same method to $H_3^+$ [17], where they showed that modeling the non-adiabatic corrections through this scaling significantly improves the first principles calculation of the rotation–vibration energies of $H_3^+$. However, it is also important to note that this scaling may be less effective as the vibrational excitation increases [29].

We have included non-adiabatic corrections in the nuclear problem by introducing a mass scaling for the H and D nuclear masses, using the same scaling relation as that proposed by Polyansky and Tennyson [17]. The resulting masses, also referred to as *intermediate masses*, are $m_H^{(i)} = 1.0075372\,\mathrm{u}$ and $m_D^{(i)} = 2.0138140\,\mathrm{u}$, compared with the nuclear masses $m_H^{(n)} = 1.00727647\,\mathrm{u}$ and $m_D^{(n)} = 2.0135532\,\mathrm{u}$. This correction is implemented

by simply replacing the nuclear masses with the intermediate masses in the nuclear Hamiltonian.

The effect of this mass scaling on the energy levels was evaluated perturbatively. The system's kinetic energy for each calculated state $v$, $K_v$, is obtained as the difference between the total and potential energy:

$$K_v = E_v - \langle V \rangle_v, \tag{1}$$

where $E_v$ is the energy of the $v$th state, and $\langle V \rangle_v$ is the mean value of the potential energy $V$ for the same state.

The kinetic energy depends on the reduced mass $\mu$, which is a function of the nuclear masses. $\mu$ then depends on the choice of the coordinate system, and a general expression is presented in [20]. In our specific case we have

$$\mu^{-1} = \frac{(1+g^2)}{m_{\mathrm{D}}} + \frac{(1-g)^2}{m_{\mathrm{H}}}, \tag{2}$$

where $g$ is a function of the two nuclear masses:

$$g = \frac{1 - \sqrt{m_{\mathrm{H}}/(m_{\mathrm{H}} + 2m_{\mathrm{D}})}}{1 + \sqrt{m_{\mathrm{H}}/(m_{\mathrm{H}} + 2m_{\mathrm{D}})}}. \tag{3}$$

The kinetic energy is inversely proportional to $\mu$:

$$K_v^{(0)} = \mu K_v, \tag{4}$$

therefore, the non-diagonal BO correction to the $v$th level $\Delta E_v$ can be evaluated using this method straightforwardly:

$$\begin{aligned} \Delta E_v &= \left(\frac{1}{\mu^{(\mathrm{i})}} - \frac{1}{\mu^{(\mathrm{n})}}\right) K_v^{(0)} = \left(\frac{\mu^{(\mathrm{n})} - \mu^{(\mathrm{i})}}{\mu^{(\mathrm{i})}\mu^{(\mathrm{n})}}\right) K_v^{(0)} \\ &= \delta_\mu \frac{K_v^{(0)}}{\mu^{(\mathrm{i})}} = \delta_\mu K_v, \end{aligned} \tag{5}$$

where $\mu^{(\mathrm{i})}$ and $\mu^{(\mathrm{n})}$ are the reduced masses calculated from equation (2) using intermediate and nuclear masses, respectively. Using the values for the nuclear masses indicated above, we obtain $\delta_\mu = -1.61 \times 10^{-4}$, which justifies the perturbative approach adopted.

In this fashion the influence of the non-BO correction was calculated, for all levels, giving an average of $1.88\,\mathrm{cm}^{-1}$ with a maximum of $2.43\,\mathrm{cm}^{-1}$ for $A_1$ states, while for $B_1$ states the average energy difference was $1.68\,\mathrm{cm}^{-1}$ with a maximum difference of $2.47\,\mathrm{cm}^{-1}$.

If such corrections were to be evaluated more carefully, one should consider the coupling among all the PESs. In particular, one expects the failures to the BO approximation to be more important for those vibrational states which have a significant amplitude in those regions of the nuclear geometries where two or more PESs come close to each other.

The $H_3^+$ system has an avoided crossing between the $1^1A'$ ground state PES and the $2^1A'$ first excited state, which are associated with the $X_2 + X^+$ and $X_2^+ + X$ dissociation channels, respectively. The crossing is located at configurations with $r \simeq 2.5a_0$ and $R \geq 8.0a_0$ [26] in dissociation coordinates where $r$ is the distance between the $X_2$ diatom nuclei and $R$ is the distance from its centre of mass to the third nucleus. The crossing is caused by the fact that, at large diatomic distances, $X_2^+ + X$ becomes the lowest dissociation channel. However, at these nuclear configurations the bound states of $D_2H^+$ have a very low amplitude (as can be seen from figure 3) because the dissociation energy of $D_2H^+$ for its lowest dissociation channel ($D_2 + H^+$) is around $15\,000\,\mathrm{cm}^{-1}$ below the required energy to reach the avoided crossing. Figure 3 in [26] depicts the crossing's potential region in detail.

## 5. Conclusion

In this paper we extend previous calculations for the vibrational band origins of $H_3^+$ to the less symmetric isotopologue $D_2H^+$. The bound states of this molecule are computationally more difficult to converge as the spectrum is more dense. We have achieved sub-wavenumber convergence for 1209 $A_1$ and 1078 $B_1$ calculated band origins up to dissociation.

At high energy, the bound states seem to show some interesting properties. In particular, there seems to be a class of states, named AVS previously [11], whose wavefunctions exhibit particularly large amplitude at large values of the ion–diatom dissociating coordinate. In order to obtain convergence for those extended states and the inner ones, we required a very large basis set which results in a very expensive calculation. It is likely that the potential used will support further bound states which extend beyond the range of our DVR grid.

Following the work in [26] we have evaluated some corrections to the Born–Oppenheimer energies. However, the correction surfaces available in [26] are only well defined in a range which is far smaller than the extent of the higher lying states, therefore we could not use them. We expect the combined relativistic and adiabatic corrections to the vibrational band origins to be of the order of magnitude of $1\,\mathrm{cm}^{-1}$. Using the mass scaling model we have also evaluated the non-adiabatic BO corrections perturbatively. For $D_2H^+$, those corrections have a lower symmetry than the potential, therefore are expected to be larger, however the simple model

employed yielded an average correction of $1.79\,cm^{-1}$ for all the calculated levels. We expect this model to be correct to better than a factor of 2, as the calculated states have a particularly low amplitude in the area where the two lowest PESs come close to each other. Finally, it is known that the higher energy states are sensitive to details of the PES. Both the fitting error and the intrinsic accuracy of the electronic structure calculations are only about $5\,cm^{-1}$ in this region [2]; these residual errors therefore remain more important than the corrections to the non-relativistic BO Hamiltonian.

Semi-classical studies of the spectrum of $D_2H^+$ near its dissociation limit can be found in the literature [30–35], but, to our knowledge, no quantum mechanical studies have been reported so far.

Heilliette and co-workers [36] studied $NO_2$ in the near dissociation region. They found, in addition to the strongly coupled three-body states, a family of states corresponding to orbiting motion of the two fragments around each other. They compared a fully quantum-mechanical treatment with a semi-classical approach and found that, whereas for the 2D case, that is with the diatom frozen, the two give similar results, the semi-classical approach fails completely in the proximity of the dissociation limit in the 3D case. This is because of the quantum character of the diatom fragment. However, as we have shown, a full quantum-mechanical treatment of the molecule in 3D near dissociation meets with great numerical difficulties and requires the use of powerful supercomputers.

Finally, it is interesting to discuss how our theoretical work relates to the spectra of Carrington *et al*. [6]. Firstly, a large increase in the density of states near dissociation is necessary to explain the exceptionally large number of lines recorded in the experiment. The low $C$ rotational constant values could lead to significantly more AVS when rotations are considered. It is possible that, associated with the AVS states, there will be a series of resonant states above dissociation. It is possible to study such states using $\mathcal{L}^2$ methods such as the Complex Absorbing Potential method [37, 38]. An analysis in this sense is currently underway, however our preliminary results show that the lifetimes associated with those purely vibrational resonances ($J=0$) are far too short for those states to be involved in Carrington *et al*.'s spectra. This is also consistent with the previous supposition that the resonances involved in the Carrington *et al*. spectra are highly excited rotational states trapped behind rotational barriers [15, 30]. A study of $H_3^+$ and $D_2H^+$ with $J \neq 0$ is also underway, but for rotationally excited calculations the numerical difficulties, represented by basis sets size, computational time and cost, increase at best linearly with $J$.

**Acknowledgement**

This work was performed as part of EPSRC's ChemReact computing consortium.

**References**

[1] J. Tennyson, M. A. Kostin, H. Y. Mussa, O. L. Polyansky, and R. Prosmiti, Phil. Trans. R. Soc. Lond. A **358**, 2419 (2000).
[2] O. L. Polyansky, R. Prosmiti, W. Klopper, and J. Tennyson, Molec. Phys. **98**, 261 (2000).
[3] P. Drossart, J. P. Maillard, J. Caldwell, S. J. Kim, J. K. G. Watson, W. A. Majewski, J. Tennyson, S. Miller, S. Atreya, J. Clarke, J. H. Waite Jr, and R. Wagener, Nature **340**, 539 (1989).
[4] A. Carrington, J. Buttenshaw, and R. A. Kennedy, Molec. Phys. **45**, 753 (1982).
[5] A. Carrington and R. A. Kennedy, J. chem. Phys. **81**, 91 (1984).
[6] A. Carrington, I. R. McNab, and Y. D. West, J. chem. Phys. **98**, 1073 (1993).
[7] M. J. Bramley, J. W. Tromp, T. Carrington Jr, and G. C. Corey, J. chem. Phys. **100**, 6175 (1994).
[8] V. A. Mandelshtam and H. S. Taylor, J. chem. Soc. Faraday Trans. **93**, 847 (1997).
[9] J. J. Munro, J. Ramanlal, J. Tennyson, and H. Y. Mussa, Molec. Phys. **104**, 115 (2006).
[10] E. Pollak and C. Schlier, Accts Chem. Res. **22**, 223 (1989).
[11] J. J. Munro, J. Ramanlal, and J. Tennyson, New J. Phys. **7**, 196 (2005).
[12] J. Tennyson, P. Barletta, J. J. Munro, and B. C. Silva, Phil. Trans. R. Soc. A (2006).
[13] B. M. Dinelli, C. R. Le Sueur, J. Tennyson, and R. D. Amos, Chem. Phys. Lett. **232**, 295 (1995).
[14] C. F. Giese and W. R. Gentry, Phys. Rev. A **10**, 2156 (1974).
[15] M. Berblinger, E. Pollak, and C. Schlier, J. chem. Phys. **88**, 5643 (1988).
[16] R. J. Le Roy, University of Waterloo Chemical Physics Research Report, CP-655 (2005).
[17] O. L. Polyansky and J. Tennyson, J. chem. Phys. **110**, 5056 (1999).
[18] H. Y. Mussa and J. Tennyson, Comput. Phys. Commun. **128**, 434 (2000).
[19] B. T. Sutcliffe and J. Tennyson, Int. J. quant. Chem. **39**, 183 (1991).
[20] J. Tennyson, M. A. Kostin, P. Barletta, G. J. Harris, J. Ramanlal, O. L. Polyansky, and N. F. Zobov, Comput. Phys. Commun. **163**, 85 (2004).
[21] J. C. Light and Z. Bačić, J. chem. Phys. **87**, 4008 (1987).
[22] J. R. Henderson and J. Tennyson, Molec. Phys. **69**, 639 (1990).
[23] A. Ernesti and J. M. Hutson, Chem. Phys. Lett. **222**, 257 (1994).
[24] D. J. Nesbitt and R. Naaman, J. chem. Phys. **91**, 3801 (1989).
[25] A. Messiah, *Quantum Mechanics* (Dover Publications, Inc., New York, 1999).
[26] R. Prosmiti, O. L. Polyansky, and J. Tennyson, Chem. Phys. Lett. **273**, 107 (1997).
[27] D. W. Schwenke, J. phys. Chem. A **105**, 2352 (2001).

[28] P. R. Bunker and R. E. Moss, Molec. Phys. **33**, 417 (1977).
[29] R. E. Moss and L. Valenzano, Molec. Phys. **100**, 649 (2002).
[30] R. Pfeiffer and M. S. Child, Molec. Phys. **60**, 1367 (1987).
[31] M. Berblinger, J. M. Gomez-Llorente, E. Pollak, and C. Schlier, Chem. Phys. Lett. **146**, 353 (1988).
[32] A. Chambers and M. Child, Molec. Phys. **65**, 1337 (1988).
[33] M. Berblinger, C. Schlier, and E. Pollak, J. phys. Chem. **93**, 2319 (1989).
[34] J. M. G. Llorente and E. Pollak, J. chem. Phys. **90**, 5406 (1989).
[35] E. Pollak and C. Schlier, Accts Chem. Res. **22**, 223 (1989).
[36] S. Heilliette, A. Delon, R. Jost, S. Y. Grebenshchikov, R. Shinke, B. Abel, and J. C. Rayez, Z. Phys. Chem. **8**, 1069 (2001).
[37] J. G. Muga, J. P. Palao, B. Navarro, and I. L. Egusquiza, Phys. Rep. **395**, 357 (2004).
[38] H. Y. Mussa and J. Tennyson, Chem. Phys. Lett. **366**, 449 (2002).